Journal of Structural Geology 33 (2011) 1776–1789

Contents lists available at SciVerse ScienceDirect

Journal of Structural Geology

journal homepage: www.elsevier.com/locate/jsg

Crystal preferred orientation in peridotite ultramylonites deformed by grain size sensitive creep, Étang de Lers, Pyrenees, France

M.R. Drury [a,*], H.G. Avé Lallemant [b], G.M. Pennock [a], L.N. Palasse [a,c,1]

[a] Department of Earth Sciences, Utrecht University, PO Box 80.021, 3508 TA Utrecht, Netherlands
[b] Department of Earth Science, Rice University, 6100 Main Street, Houston, TX 77005-1892, USA
[c] Oxford Instruments Plc, Halifax Road, High Wycombe, UK

ARTICLE INFO

Article history:
Received 13 December 2010
Received in revised form
3 October 2011
Accepted 3 October 2011
Available online 12 October 2011

Keywords:
Crystallographic preferred orientation
Olivine
Grain size sensitive creep
Ultramylonite
Pyrenees
EBSD
Rheology
Deformation mechanisms

ABSTRACT

In naturally deformed upper mantle rocks a strong olivine crystallographic preferred orientation (CPO) occurs in rocks with grain sizes larger than about 15 μm. Finer grained peridotites tend to have weak to random olivine CPO. The different types of olivine CPO are usually interpreted in relation to the dominant deformation mechanisms: with a strong CPO indicating dislocation creep and a random CPO indicating grain size sensitive (GSS) mechanisms involving grain boundary sliding and diffusion creep. Here we report the occurrence of a weak but systematic olivine CPO in ultra-fine-grained (0.5–10 μm) ultramylonites from the Étang de Lers lherzolite, Pyrenees, France. The microstructures, with elongated grains and mixed distribution of phases in the ultramylonites indicate deformation by dominant GSS creep. In theory, an olivine CPO may develop in rocks deformed by GSS creep during dislocation accommodated boundary sliding or phase boundary controlled diffusion creep in pyroxene-rich rocks. Alternatively, the CPO may be a relict texture preserved because the elongated grain shapes limit rotation during grain boundary sliding. Our observations confirm theoretical and experimental studies, which predict that systematic CPO and an associated seismic anisotropy can occur in naturally deformed upper mantle rocks during deformation by grain boundary sliding and diffusion creep.

1. Introduction

The crystallographic preferred orientations (CPO) in naturally and experimentally deformed upper mantle rocks have been studied extensively with the goal of understanding the deformation processes and seismic anisotropy of the upper mantle (Den Tex, 1969; Avé Lallemant and Carter, 1970; Nicolas, 1986; Ben Ismail and Mainprice, 1998; Jung and Karato, 2001). The main types of CPO in peridotite mylonites and tectonites are well known in rocks with grain sizes large enough to be measured using light microscopy and U-stage measurements. Coarse grained olivine rocks usually have strong CPOs, which can be divided into a number of types that reflect different deformation conditions and deformation modes (Mainprice and Nicolas, 1989; Jung and Karato, 2001). The application of electron backscattered diffraction (EBSD) enables the CPO in very-fine grained olivine rocks to be investigated (Fliervoet et al., 1999; Faul and Fitz Gerald, 1999). Studies of the olivine CPO in many peridotite mylonites, have found weak to random CPOs in rocks with grain size less than about 15 μm (Newman et al., 1999; Dijkstra et al., 2002; Michibayashi and Mainprice, 2004; Warren and Hirth, 2006; Toy et al., 2010). Such random CPOs in very highly deformed rocks have been interpreted as evidence for the operation of grain size sensitive (GSS) creep.

Some of the finest grained mantle rocks ever reported occur in thin vein-like ultramylonite zones in the peridotites from the Northern Pyrenees (Avé Lallemant, 1967; Fabriès et al., 1991; Vissers et al., 1997). These rocks have grain sizes less than 10 microns, yet light microscopy observations on ultramylonites from Étang de Lers (Avé Lallemant, 1967) suggest that there is a clear preferred crystal orientation: Avé Lallemant (1967) noted that " ……a pronounced preferred orientation of olivine and possibly enstatite is visible under the microscope upon insertion of the gypsum plate. Inspection of several sections suggests a strong [010] point maximum perpendicular to the ultramylonite zone". A pronounced CPO like this is unexpected in rocks that are so fine-grained that they are likely to have deformed by GSS creep. The objective of this study is to measure and quantify the CPO and microstructures in these ultra-fine grained vein-like ultramylonites. The narrow vein-like appearance of these ultramylonites

* Corresponding author. Fax: +31 30 2537725.
E-mail address: M.R.drury@uu.nl (M.R. Drury).
[1] Present address: Bruker AXS Nanoanalysis, Berlin.

0191-8141/$ – see front matter © 2011 Elsevier Ltd. All rights reserved.
doi:10.1016/j.jsg.2011.10.002

zones suggest they may have initiated as cataclastic fractures or pseudotachylites (Vissers et al., 1997), although no pseudotachylites or injection veins have been found in the Pyreneean peridotites. The strong internal foliation and spectacular development of asymmetric clast systems (Avé Lallemant, 1967; Vissers et al., 1997; Newman et al., 1999) shows that the ultramylonites accommodated large ductile strains, after their formation.

The terms we use to describe grain sizes and rock types follow the preferred terminology of the IUGS classification for metamorphic rocks (Fettes and Desmons, 2007). We will describe rheological regimes in terms of their grain size and stress sensitivity. In olivine and other minerals three main regimes occur, grain size insensitive (GSI) power law creep (Chopra and Paterson, 1984), grain size sensitive (near) linear creep (Karato et al., 1986) and grain size sensitive power law creep (Walker et al., 1990; Hirth and Kohlstedt, 1995). These rheological regimes are thought to correspond to different deformation mechanisms. In the GSI-power law regime dislocation creep is the dominant mechanism, in the GSS linear regime, grain boundary sliding and diffusion creep are dominant, while the GSS-power law regime is thought to be a hybrid deformation mechanism involving serial grain boundary sliding and dislocation creep on the weakest slip system in olivine (Hirth and Kohlstedt, 2003). This hybrid mechanism is often abbreviated as disGBS creep (Warren and Hirth, 2006).

2. Regional overview of the Pyrenees

The Pyrenees (Fig. 1) are a WNW-ESE -trending orogenic belt that has been divided into three sub-belts (Zwart, 1962; Choukroune et al., 1990; Barruol et al., 1998): Pyrenean Axial zone, North Pyrenean zone, and South Pyrenean zone. The contact between the Axial and Northern zone is the North Pyrenean fault zone. This three-fold division is, to a large extent, the result of Cretaceous and Tertiary orogenic processes, although the Pyrenees mountain range was also a major zone of deformation in Late Paleozoic time. Paleozoic rocks underlie most of the Pyrenees and areas to the south and north. These rocks were metamorphosed at high temperatures and relatively low pressures during the Carboniferous Hercynian (Variscan) orogeny. This event has been related to the assembly of Pangea (Weil et al., 2001).

During the Triassic to Late Jurassic, WNW-trending rift basins formed as a result of the break-up of Pangea (Yilmaz et al., 1996). A second-phase of rifting occurred in middle Cretaceous (Albian) time. This event coincided with the opening of the Bay of Biscay when the Iberian plate rotated counterclockwise away from Brittany (Van der Voo and Boessenkool, 1973; Vera, 2001). At the same time the North Pyrenean fault zone was activated as a major left-lateral strike-slip fault (Vergés and García Senz, 2001; Vera, 2001).

During Late Cretaceous and Early Tertiary time Iberia was moving northward and collided with the European block. This resulted in the "Pyrenean" fold and thrust belt (Van der Voo and Boessenkool, 1973; Choukroune et al., 1990; Vergés and García Senz, 2001; Larrasoaña et al., 2003). At this time the North Pyrenean fault may have become a right-lateral shear zone (Sibuet et al., 2004).

Interpretation of the deep seismic reflection profile through the central part of the Pyrenees (Choukroune et al., 1990) suggests that Iberia was subducted to the north beneath the European plate. It caused the formation of a relatively wide south-vergent fold and thrust belt in the south. The Pyrenean axial zone (Zwart, 1962; Vissers, 1992) seems to be uplifted in a major antiformal duplex. The overthrusting caused the foreland to subside, forming the Ebro Basin. A much less significant north-vergent fold and thrust belt formed to the north, also causing subsidence and the formation of the Aquitaine Basin (Choukroune et al., 1990). The thrusting was accompanied by displacements along the North Pyrenean fault zone suggesting that displacement partitioning was occurring (Avé Lallemant and Oldow, 2000).

2.1. North Pyrenean metamorphic zone

The southern part of the North Pyrenean zone (Fig. 1) is called the North Pyrenean metamorphic zone (Fabriès et al., 1991). It is a relatively narrow belt (0.5 to several kilometers) consisting of highly deformed and metamorphosed Triassic to Cretaceous sedimentary rocks (mainly carbonates) and fragments of Paleozoic crystalline and ultramafic rocks (Casteras, 1933; Ravier, 1959; Zwart, 1962; Choukroune et al., 1990; Fig. 1). The metamorphism occurred at high temperatures and low pressures (Ravier, 1959; Minnigh et al., 1980) during middle Cretaceous time as evidenced by $^{40}Ar/^{39}Ar$ and Rb/Sr ages (104–92 Ma; Albarède and Michard-Vitrac, 1978).

Almost all rocks in the metamorphic zone are strongly brecciated. Fragments in the breccia are generally angular. The structures in the large lherzolite bodies suggest that they are fragments and

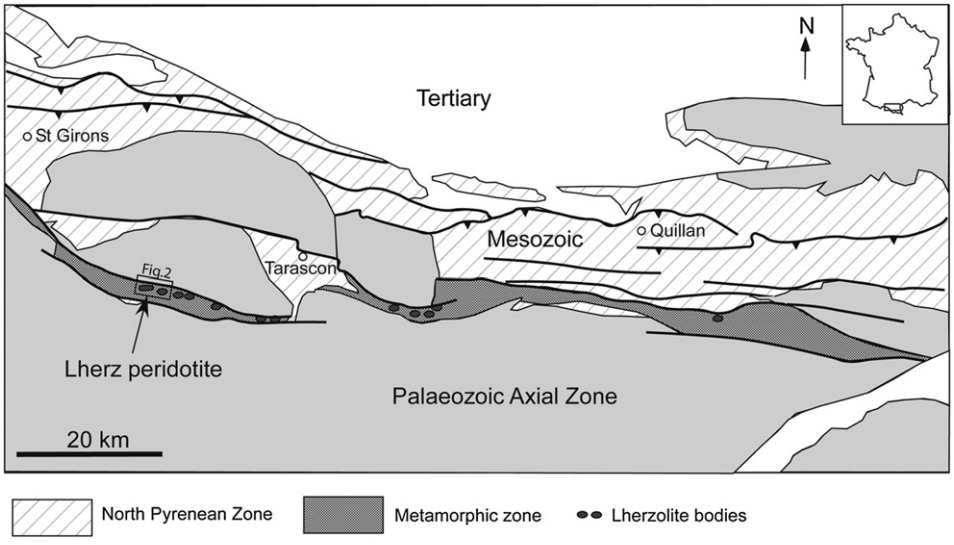

Fig. 1. Simplified geological map of part of the North Pyrenees, after Choukroune and Seguret (1973). Lherzolite bodies occur in the North Pyrenean metamorphic zone that occurs in the southern part of the Mesozoic North Pyrenean zone, north of the Paleozoic axial zone. Rectangle outlines the area of Fig. 2.

not connected at depth to each other (Avé Lallemant, 1967). These breccias occur generally in areas where the metamorphism was most intense (Minnigh et al., 1980). The brecciation and the metamorphism may in part be related to the ascent of the ultramafic rocks to the surface of the earth. Some of the breccias have recently been shown to be sedimentary rocks containing peridotite detritus, suggesting that upper mantle rocks were locally exposed at the floor of pull-apart rift basins (Lagabrielle and Bodinier, 2008: Lagabrielle et al., 2010).

2.2. Ultramafic bodies

One of the largest ultramafic bodies is exposed around the Étang de Lers (the type locality of lherzolite). It has a rectangular shape with the EW trending longest dimension of 1.6 km, and the shortest of 0.7 km (Fig. 2). The ultramafic rocks at Étang de Lers are mostly lherzolite, with lesser amounts of harzburgite, dunite, garnet pyroxenite, spinel pyroxenite, amphibolite, hornblende veins, ultramylonites, and serpentinites (Lacroix, 1894; Casteras, 1933; Ravier, 1959; Avé Lallemant, 1967; Le Roux et al., 2007). Henry et al. (1998) presented numerous $^{40}Ar/^{39}Ar$ and Sm/Nd ages of the pyroxenites and lherzolites; they show a bimodal distribution: Paleozoic (297–536 Ma) and Cretaceous ones (114–101 Ma). Thus, it appears that the lherzolite bodies were emplaced in middle Cretaceous time.

The lherzolites have a well-developed pyroxenite layering, which is folded into open to isoclinal folds with wavelengths of a few centimeters to several meters (Avé Lallemant, 1967). Flattened and elongate spinel grains give rise to a foliation parallel to the fold axial planes and a stretching lineation parallel to the fold axes (Avé Lallemant, 1967). Most lherzolites of the Étang de Lers complex are quite homogeneous, have only a few percent of very-fine-grained crystals (about 50 μm) along the boundaries of medium-grained porphyroclasts (up to about 4 mm), and have a strong shape preferred orientation defined mainly by elongated olivine. The foliation in the lherzolite may have formed initially at 1.5–1.8 GPa and temperatures >950 °C (Fabriès et al., 1998; Le Roux et al., 2008). This foliation is overprinted by thin (2–10 mm thick), ultra-fine-grained (<10 μm) ultramylonite zones (Fig. 2) and serpentine veins, which are formed at lower temperatures and depths (Vissers et al., 1997; Fabriès et al., 1998). The vein-like ultramylonites may have initiated as brittle structures (Vissers et al., 1997).

3. Present study of the ultramafic ultramylonites at Étang de Lers

3.1. Methods

The microstructures and lattice preferred orientations have been studied in oriented sections taken from large hand specimens. Microstructures were studied using polarized light microscopy and backscattered electron imaging in the Scanning Electron Microscope (SEM). Semi-quantitative phase discrimination was based on Energy Dispersive (ED) X-ray analyses using electron beam conditions of 10–20 kV and a range of spot sizes to reduce the deadtime of the analysis. The CPO were studied using a light microscope equipped with a four axes universal stage and EBSD in the SEM using electron beam conditions of 20 kV, spot size 5, and a 50 micron aperture. Grain orientations using EBSD were

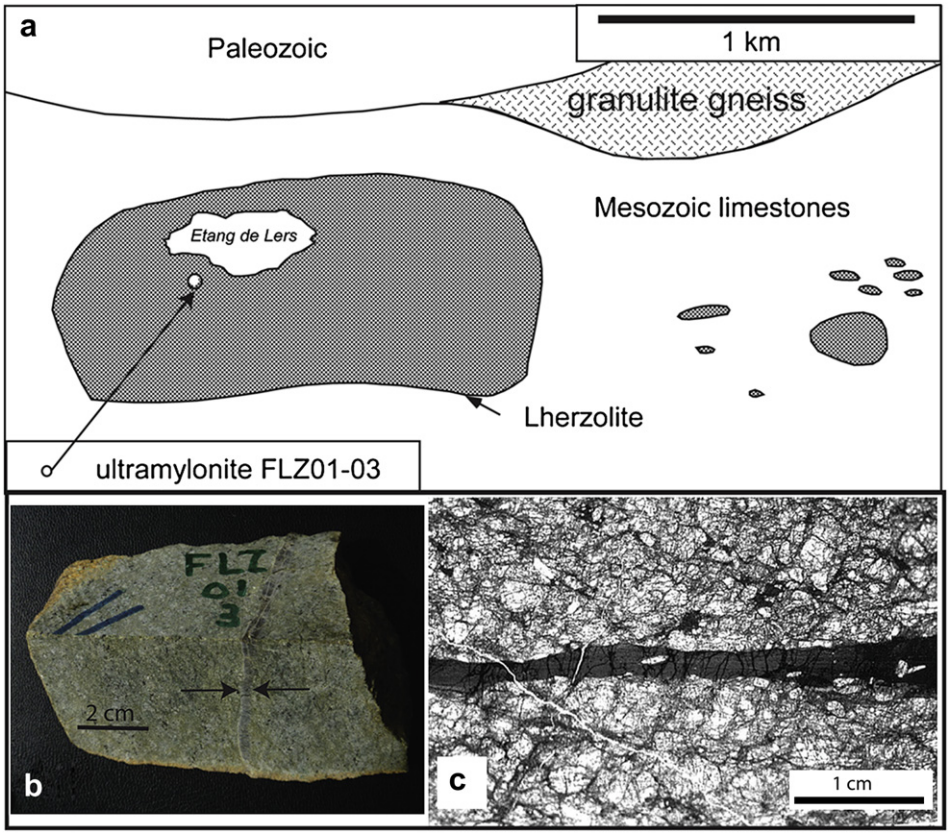

Fig. 2. (a) Simplified geologic map of the Étang de Lers area after Avé Lallemant (1967). Sample locality indicated by white dot. (b) Photograph of sample FLZ01-03 showing thin ultramylonite zone (arrowed). (c) Digital scan of thin section showing ultramylonite zone.

determined interactively with one measurement per grain. The grains were identified in forward-scattered electron images. Automatic indexing worked well for most olivine grains while most pyroxene grains were indexed manually. All solutions were checked for mis-indexing caused by hexagonal pseudosymmetry of olivine (Fliervoet et al., 1999). EBSD mapping was used for detailed analysis of some areas. Automatic indexing provided reasonable results for olivine but variable results for pyroxenes and the minor phases in the mylonites. EBSD maps were processed to remove single spikes, and to replace non-indexed points surrounded by six nearest neighbors of similar orientation. In addition common mis-indexing of olivine such as a 60° rotation around [100] (Fliervoet et al., 1999) were removed. We used a FEI-Company XL30-SFEG SEM equipped with Oxford Instruments HKL Technology Channel 5 software.

3.2. Results

The vein-like ultramylonites occur sporadically throughout the Lers peridotite and make up a very small volume fraction of the body. In one outcrop of the Étang de Lers (GPS UTM co-ordinates 31T 0367143/4740619, map datum WGS84) two samples (FLZ-01-2 and FLZ-01-3) were collected a few meters apart that contained thin ultramylonite zones (Fig. 2). These samples consist of three rock types: (1) medium-grained foliated lherzolite, (2) ultra-fine-grained lherzolitic ultramylonite, and (3) serpentinite veins and joints. The olivine microstructures in the two foliated lherzolites are similar and are also almost identical to the microstructures of twenty foliated lherzolite samples, described by Avé Lallemant (1967). Therefore, we discuss only the results of one of the samples (FLZ-01-3).

3.2.1. Foliated lherzolite

The foliated lherzolitic wall rock, host to the ultramylonites, contains about 75% olivine, 20% orthopyroxene, 5% clinopyroxene, and traces of spinel and amphibole. The samples are mildly serpentinized (~5%). The olivine has a strong bimodal grain-size distribution. The large grains are about 4 mm long parallel to the mineral lineation and 2 mm wide, perpendicular to the foliation. The small olivine grains are equant and less than 100 μm in diameter, most are less than 10 μm. The very-fine-grained matrix often occurs in relatively straight bands along the margins of the porphyroclasts (Vissers et al., 1997). The large olivine grains have zones of undulatory extinction, and, locally, sharp kink bands and sub-grain boundaries parallel to (100). Orthopyroxene and clinopyroxene have an interstitial habit and have a grain size of about 1.5 mm. Orthopyroxenes have sharp kink bands normal to [001]. Clinopyroxenes are undeformed or have patchy undulatory extinction. The rare, brown-amphibole grains attain a size of 75 μm; they occur in the neighborhood of the ultramylonites; sections taken more than 15 cm away from the ultramylonite are amphibole-free. Spinel grains are generally about 0.4 mm long, but a few grains are up to 1.5 mm in size.

In the lherzolitic wall rock (sample FLZ-01-3), the orientation of the optical indicatrix axes of 80 olivine grains were obtained (Fig. 3A). They have a strong [100] CPO parallel to the lineation and a [010] maximum at high angle to the foliation plane.

3.2.2. Ultramylonite

The ultramylonites in the Étang de Lers area have variable thicknesses of between 2 and 10 mm. However, there can be rather extensive cross-cutting of the foliated lherzolites for tens of meters.

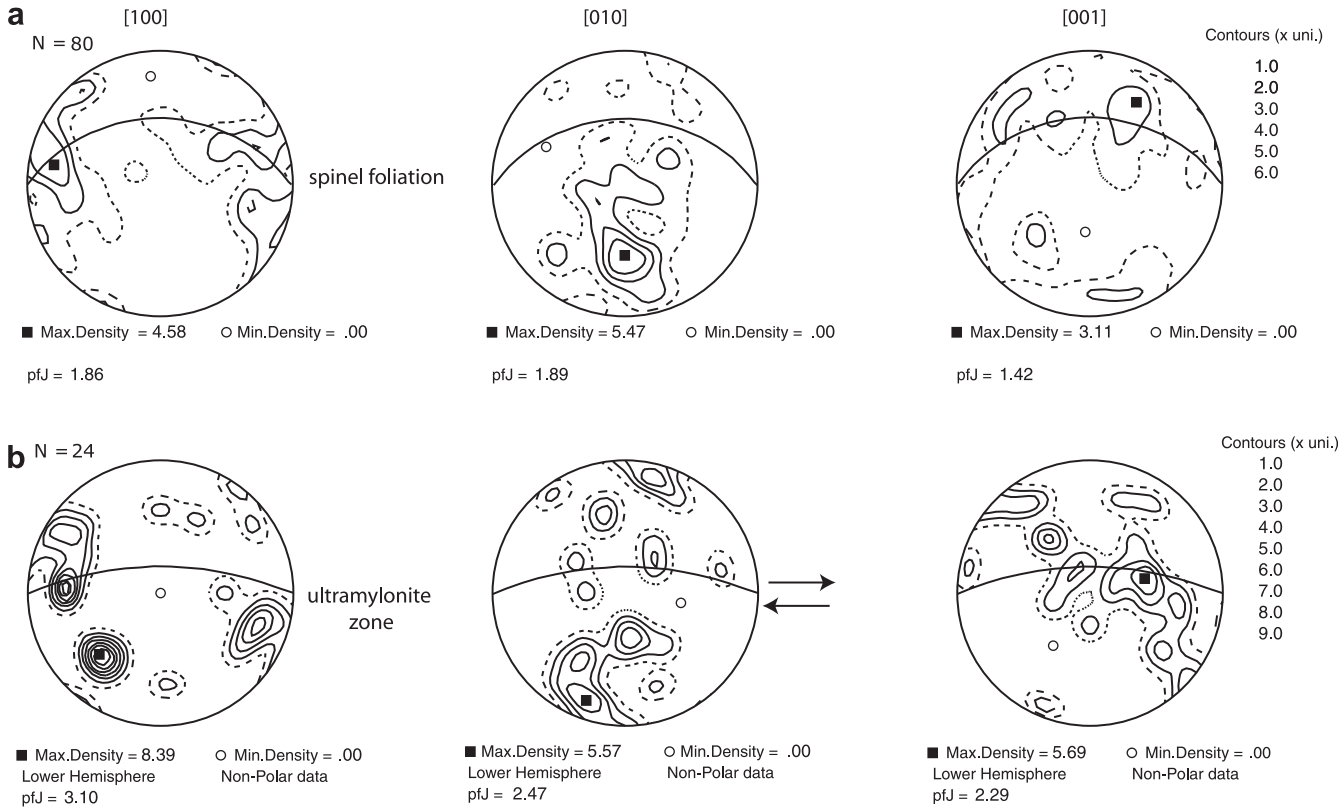

Fig. 3. (a). Equal-area, lower-hemisphere projections of 80 grains showing the [100], [010], and [001] olivine axes in foliated lherzolite sample FLZ-01-3. (b). Equal-area, lower-hemisphere projections of 24 grains showing the [100], [010], and [001] axes of porphyroclastic olivine grains in the ultramylonite in sample FLZ-01-3. Geographic orientation of ultramylonite foliation is N54E38S and the lineation is S20W23. In the reference frame of the thin section the foliation has near vertical dip and east-west strike, and the lineation is east-west and horizontal. Contours are in multiples of uniform distribution.

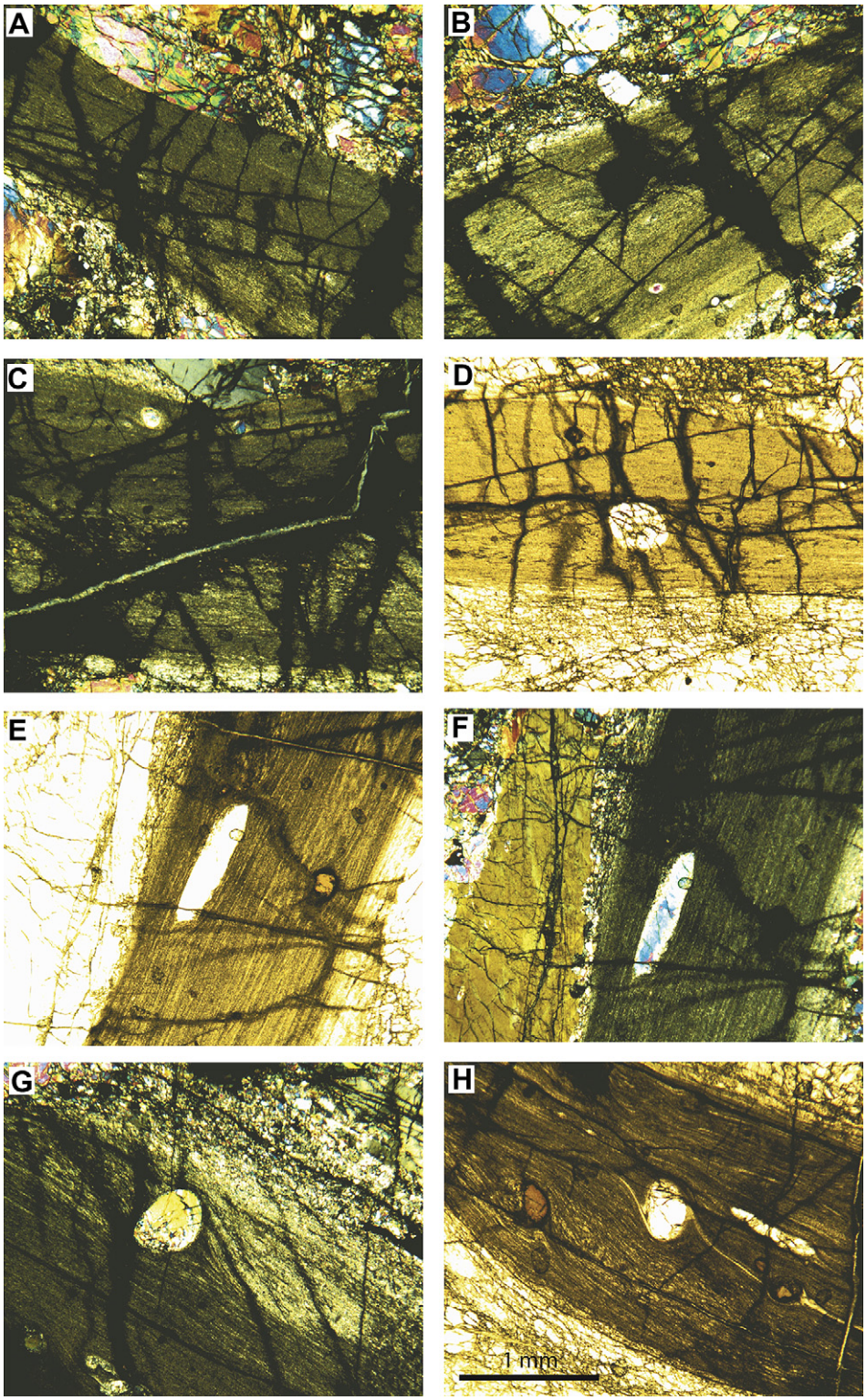

Fig. 4. Photomicrographs of ultramylonite of sample FLZ-01-3. Figures a, b, c, f, and g are taken with crossed polars, and d, e, and h with plane-polarized light. EW dimension in all figures is about 3 mm. All shear sense indicators show the same shear sense, which is sinistral in these images of the section plane and top to the north in geographical co-ordinates. (a). Ultramylonite layer trending N60W, cutting across coarse-grained foliated lherzolite; N20E trending serpentine veins do not generally propagate into foliated lherzolite; N80W trending fractures may be Riedel shears. (b). Same as A, but differently oriented. (c). Ultramylonite layer is EW oriented; N75E vein (Riedel shear) cross-cuts layer-perpendicular serpentine veins. (d). Riedel shears trending N75E, cross-cutting NS trending veins. (e) and (f). Shows olivine σ clasts in ultramylonite; note coarsening of grains in the margin of the ultramylonite zone, toward the contact with the wall rock. (g). Clinopyroxene porphyroclast in centre. Note coarsening of matrix toward the foliated lherzolite – ultramylonite contact. (h). Spinel σ clasts and olivine δ clast.

The thickness of the ultramylonites varies along the length of the zone (Figs. 2C and 4A). Planar bands of fine grains in the wall rock (Vissers et al., 1997) link into the ultramylonite band at points where the ultramylonite band is thickest. These planar bands have a Riedel orientation with respect to the ultramylonite band. The ultramylonites are parallel to the foliation in the lherzolites or cross cut the foliation at small angles. The ultramylonites are seen to cross cut and displace the pyroxenite layering. The lineations in the ultramylonite are sub-parallel to the lineations in the wall rock.

The ultramylonites have an ultra-fine grained matrix with large elliptical porphyroclasts of ortho- and clinopyroxene, olivine, spinel, and brown-amphibole. In thin section the matrix is almost opaque, but some banding is visible parallel to the ultramylonite walls (Fig. 4). Generally, the ultramylonite zones cut across the porphyroclastic wall rock with a straight sharp boundary but in places there is a gradient of grain size from ~4 mm to ~10 μm.

The porphyroclasts are generally ellipsoidal in shape with the long axis at an angle to the ultramylonite layers. Most porphyroclasts have asymmetric tails of both the σ- (Fig. 4E, F) as well as the δ-type (Fig. 4H) (Passchier and Trouw, 1996). These structures show consistently the same, top to the north, sense of shear.

In sample FLZ-01-3, the orientation of 24 olivine porphyroclasts was measured (in six parallel thin sections). The CPO (Fig. 3B) is somewhat different from the CPO in the lherzolite. There is a [010] maximum parallel to the [010] CPO in the lherzolite, and a [100] point maximum parallel to the [100] in the lherzolites. However, there is a second [100] maximum in the ultramylonite that does not occur in the lherzolites and the [001] poles are spread out along a girdle that is oblique to the ultramylonite foliation.

3.2.3. *Microstructure and mineralogy of ultramylonite*

In the outer rim of the ultramylonite a foliation is present, defined in light microscopy by coarser translucent and finer less translucent bands (Fig. 4E, G). Boundaries between different bands are relatively straight and continuous parallel to the ultramylonite plane. At the margin of the ultramylonite zone there are bands sub-parallel to the margin (Fig. 5) in which the grain size abruptly decreases. The grain size is 200–100 μm in the first band, 10–20 μm in the second band, and 0.5–10 μm at the edge of the ultramylonites. Within the ultramylonite band the grains are equant, to highly elongated, with a good alignment of grain and phase boundaries. Many phase boundaries, particularly those between olivine and orthopyroxene, have low amplitude cusps and bulges along them (Fig. 6).

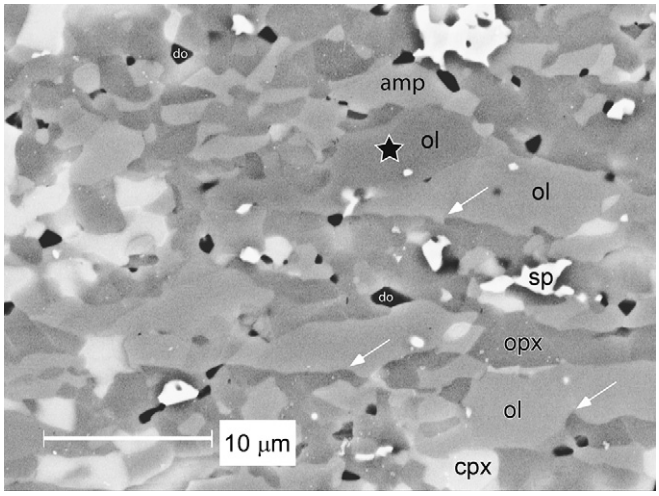

Fig. 6. Backscattered electron SEM image of microstructure in core of the ultramylonite zone. Large grains of olivine (ol) and orthopyroxene (opx) are elongated parallel to the foliation. Other minerals include clinopyroxene (cpx) amphibole (amp) and spinel (sp). The arrow shows an example of a long olivine-orthopyroxene boundary with local cusps and bulges. The small (0.5–2.0 μm) dark grains are dolomite (do). The star marks a reference grain in the EBSD map of Fig. 9.

The matrix mineral assemblage in the ultramylonite was identified using both ED X-ray analysis and EBSD. The matrix consists of olivine, ortho- and clinopyroxene, spinel, and amphibole (Figs. 6 and 7) with a mean grain size of 2–3 μm perpendicular to the foliation, and 4–5 μm parallel to foliation. A carbonate phase, dolomite, is also present, with approximate Ca/(Ca + Mg) ratio of 0.44–0.45 (Fig. 7A). A few grains of andesine plagioclase (An 38–40) occur at the rim of spinel porphyroclasts (Fig. 7C) and more rarely within the ultramylonite matrix.

Manual EBSD measurements in several areas in the ultramylonite showed a weak CPO of olivine and orthopyroxene in the ultramylonite zone (Fig. 8). The CPO of the bands within the ultramylonite zone varies slightly between the different bands. In olivine the [010] axes have a maximum normal to the foliation with [001] and [100] axes in a weakly defined girdle normal to the [010]

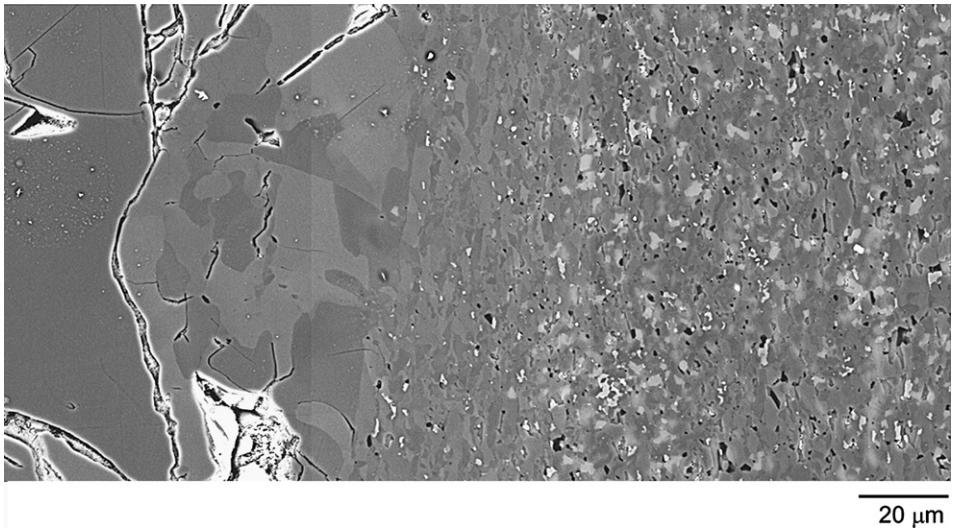

Fig. 5. Backscattered electron SEM image showing the edge of the ultramylonite zone. The grain size decreases in bands at the edge of the ultramylonite zone. The first band to the left (only one orthopyroxene grain is visible) has a grain size of 20–100 μm; the second band has a grain size of about 20 μm while the ultramylonite has a grain size of 0.5–10 μm.

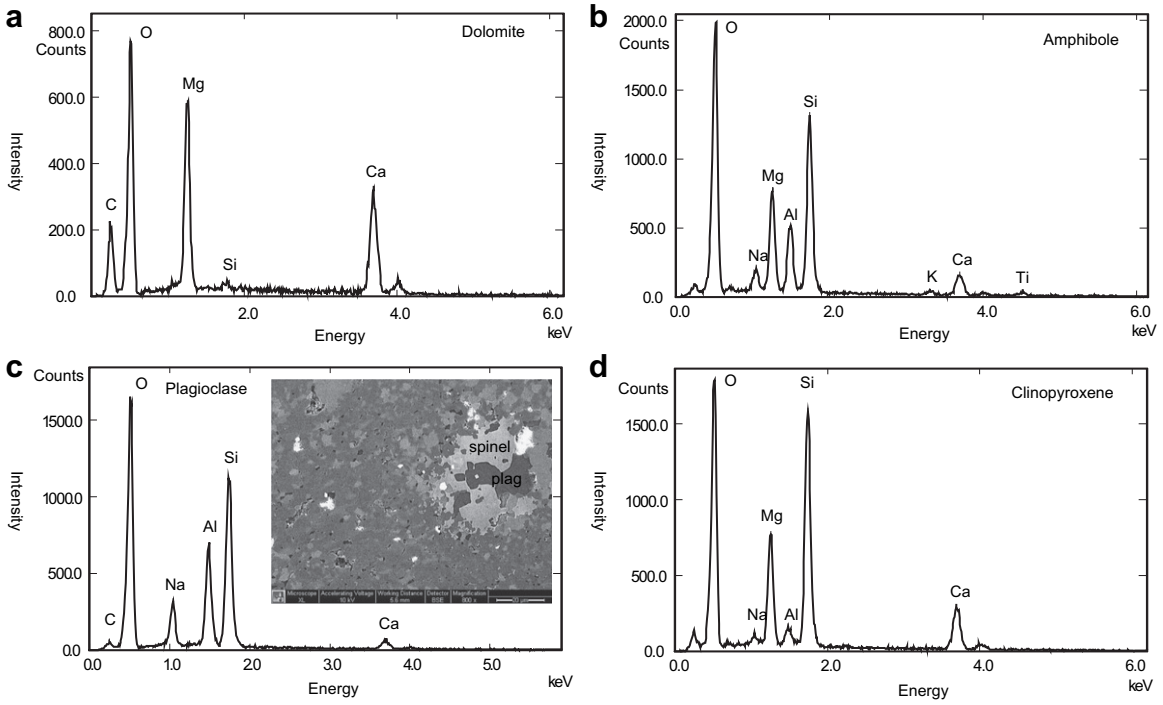

Fig. 7. X-ray spectra of minerals in the ultramylonite. (a) dolomite, (b) amphibole, (c) plagioclase, and (d) clinopyroxene. Mineral compositions were confirmed by semi-quantitative standard-less analysis.

axis maximum. The maximum density in the girdle varies from band to band in the ultramylonite zone. In one band (layer C, Fig. 8) the olivine shows a girdle distribution of [001] sub-parallel to the foliation, whereas a subset of the larger olivine grains (>3 μm) in this band have a stronger preferred orientation with a [001] axes maximum sub-parallel to the clast lineation. Orthopyroxene shows a weak preferred orientation with a [010] axes maximum at 20° from the clast lineation (Fig. 8).

The local olivine microstructure in the fine-grained ultramylonite band, in the area of Fig. 6, was studied by automatic EBSD mapping (Fig. 9). The orientation maps show that the larger olivine domains are polycrystalline with a grain size between 4 and 10 μm. There is very little lattice bending within the olivine grains and no sub-grain boundaries (misorientations more than 1°) were detected (Fig. 9).

3.2.4. Serpentine veins and joints

The ultramylonite is cross-cut by two sets of serpentine veins (Fig. 4A, B): one set of veins is at high angle to the mylonite contact and the other is at very low angle. The first veins are the oldest, as, generally, they have not propagated into the foliated lherzolite wall rock. These veins seem to indicate brittle, layer-parallel extension. As these veins occur only in the ultramylonites, the strain in the foliated lherzolite must have been taken up by more distributed deformation that may be related to serpentinization (Iyer et al., 2008). The low-angle veins extend into the foliated lherzolite and cross-cut the high angle veins. The low angle veins have a similar orientation to Riedel shears, which suggests that the serpentine veins formed during deformation, with the same shear sense as the ultramylonite.

4. Discussion

4.1. Kinematics of ultramylonite zone

The CPO in the foliated lherzolite (Fig. 3) has an orthorhombic symmetry with a [010] maximum normal to the foliation and [100] maximum parallel to the mineral lineation. On the basis of experimental work (Carter and Avé Lallemant, 1970; Zhang and Kararo, 1995; Bystricky et al., 2000) the foliation represents the XY finite strain plane, and the lineation parallels the major principal extensional strain axis X (Avé Lallemant, 1975). The CPO is not obviously asymmetric suggesting that shear strains were very high.

Only twenty-four porphyroclastic olivine grains were found in six parallel thin sections of the ultramylonite, sample FLZ-01-3. Surprisingly, the CPO of these grains is rather strong (Fig. 3B) and is similar to the CPO of the host lherzolite. All kinematic indicators in the ultramylonite show the same sense of shear sub-parallel to the [100] maximum in the lherzolite. This suggests that the structures in the ultramylonites and wall rocks have a similar shear sense (Fig. 4), which could be related to a progressive deformation history in a ductile to brittle, trans-extensional shear zone system (Fabriès et al., 1991; Vissers et al., 1997) that exhumed the mantle rocks, first to crustal depths and eventually, at the seafloor (Lagabrielle and Bodinier, 2008; Lagabrielle et al., 2010).

4.2. PT conditions and fluid infiltration of ultramylonites

The occurrence of carbonate and amphibole in the ultramylonite requires infiltration of CHO fluids. Possible reactions for the formation of dolomite are (Trommsdorff and Connolly, 1990; Connolly and Trommsdorf, 1991):

$$\text{olivine} + \text{diopside} + CO_2 = \text{orthopyroxene} + \text{dolomite} \quad (1)$$

$$\text{olivine} + \text{diopside} + \text{CHO fluid} = \text{dolomite, amphibole} + \text{orthopyroxene} \quad (2)$$

These reactions can partly explain the high orthopyroxene content in the ultramylonites. The occurrence of brown-amphibole clasts in the ultramylonite and the proto-mylonitic wall rock indicates that initial brown-amphibole growth occurred before shear

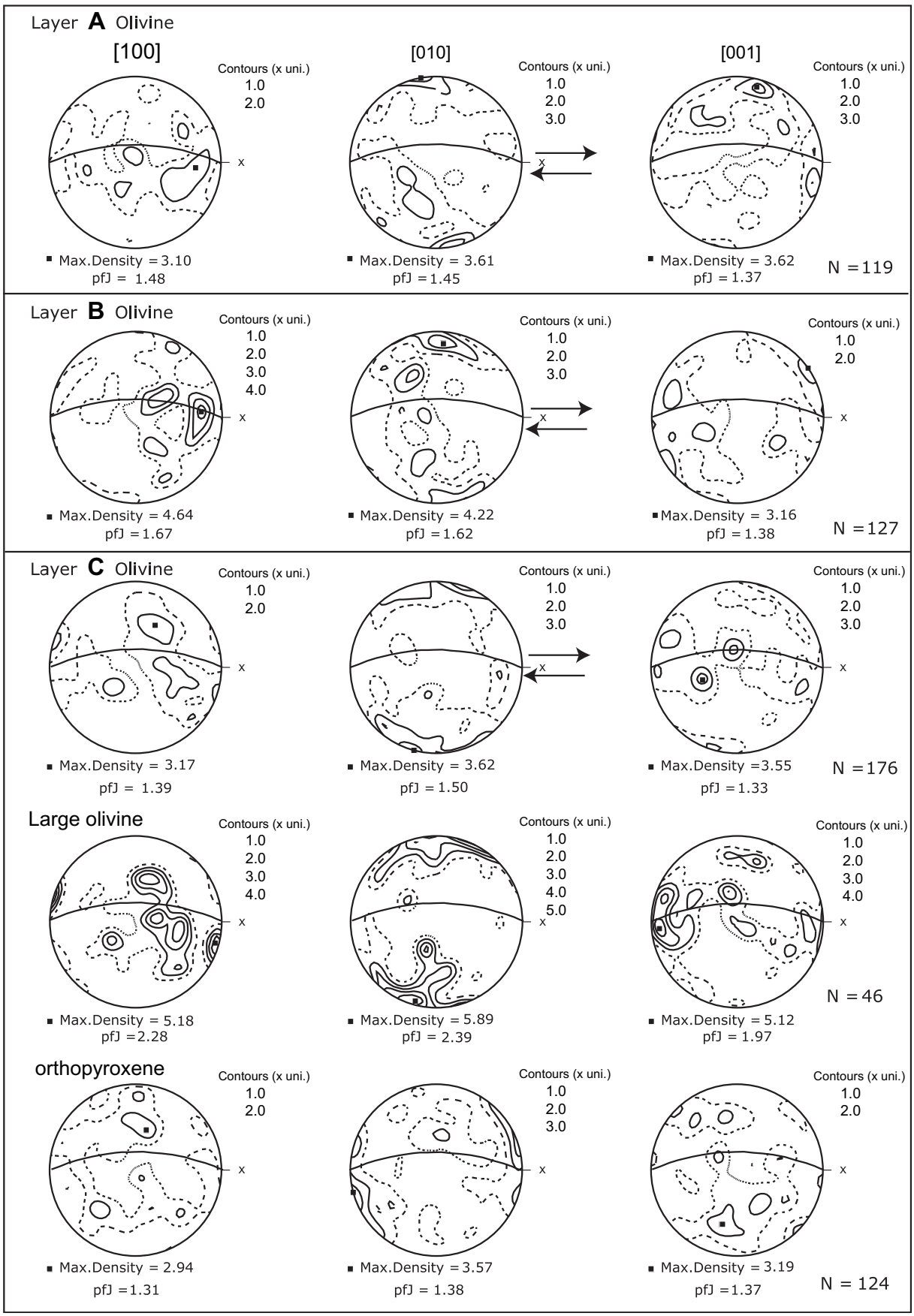

Fig. 8. CPOs determined from interactive EBSD measurements in different layers (A, B and C) of the ultramylonite zone. Layer C includes the area in Fig. 6. The CPO in layer C is displayed for all olivine grains, large olivine grains (3–10 μm) and opx grains. Olivine and orthopyroxene have a weak CPO, with olivine {010} sub-parallel to foliation. Contours are at multiples of uniform distribution.

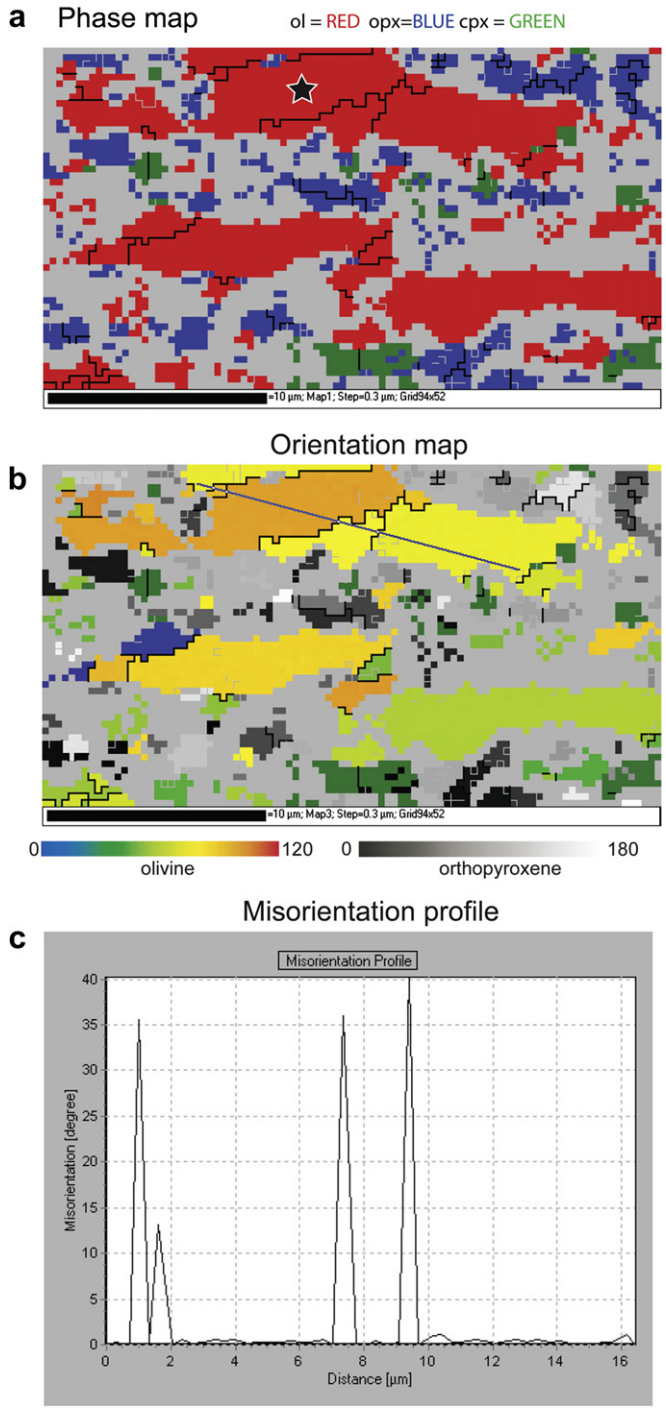

Fig. 9. Automatic EBSD map of ultramylonite microstructure in area shown in Fig. 6. (a) Phase map with olivine shown in red, orthopyroxene in blue and clinopyroxene in green. A reference grain is marked by a star in this figure and Fig. 6. (b) Orientation map of olivine showing that large elongate olivine domains are polycrystalline. Boundaries with misorientation more than 10° are shown as black lines (c) Misorientation profile along traverse shown in (b), showing the lattice rotation with respect to the previous point in the profile.

zone formation. The paragenesis of olivine, orthopyroxene, diopside, dolomite and amphibole is an univariant assemblage in the CMS-HC chemical system, which is stable at a well-defined temperature, pressure, and CO_2 rich fluid composition (Connolly and Trommsdorf, 1991). Alternatively, the occurrence of diopside and olivine may be a meta-stable assemblage that is present because insufficient fluid was available for the complete reaction. This could occur if the amount of fluid was limited to <5 wt% CO_2 and 0.4 wt% H_2O (Wyllie, 1979).

The small plagioclase grains located at the rim of spinel clasts (Fig. 7c) show: i) that the ultramylonite assemblage developed at lower pressures (0.2–0.6 GPa) than the spinel assemblage preserved in the wall rock (>0.6 GPa) and ii) that the pressure-temperature (PT) path of the Lers peridotite passed through the high temperature, low pressure, plagioclase lherzolite PT field (Bucher and Frey, 1994). The lack of plagioclase and presence of spinel and amphibole in the ultramylonite matrix is consistent with subsequent reaction of matrix plagioclase + olivine + orthopyroxene + H_2O to form amphibole and spinel.

The assemblage of orthopyroxene and dolomite is stable at temperatures less than 750 °C, for pressures less than 0.6 GPa. Furthermore, temperatures less than 700 °C are indicated if the mineral paragenesis (olivine, orthopyroxene, diopside, dolomite, and amphibole) is an equilibrium assemblage (Connolly and Trommsdorf, 1991). The estimated PT conditions for the ultramylonites are, therefore, $P < 0.6$ GPa and $T < 750$ °C, which are remarkably low pressures and temperatures for ductile deformation of mantle rocks.

The CO_2 in the Pyrenean peridotites could have been derived from the metamorphosed Mesozoic carbonate sequence, or from the crystallization of CO_2 bearing melts that originated from deeper in the upper mantle (Yaxley et al., 1991). There is evidence for the local occurrence of carbonatite metasomatism in the Lers peridotites (Woodland et al., 1996), which can be related to the crystallization of Cretaceous alkali basalt dykes (Bodinier et al., 2004). The vein-like ultramylonites were active at estimated depths of 10–20 km and temperatures of less than 750 °C. These conditions overlap with the highest temperature conditions estimated for the metamorphism of the Mesozoic carbonate sedimentary rocks during the emplacement of the peridotite bodies at middle and upper crustal depths (Golberg and Leyreloup, 1990). The presence of tremolite, found in siliceous dolomitic marbles near the Lers peridotite, indicates amphibolite grade metamorphism of the limestones in this area (Avé Lallemant, 1967; Minnigh et al., 1980). Reactions in the Mesozoic limestones, including the formation of tremolite, (Bucher and Frey, 1994) are the most likely source of the CO_2 that infiltrated into the Lers peridotites, possibly along fractures that were re-activated later to form ultramylonites (Vissers et al., 1997). It is possible that fluid infiltration occurred as the hot peridotites were exhumed along extensional shear zones and juxtaposed next to the deeper parts of the carbonate sequence.

4.3. Grain size reduction, deformation mechanisms and rheology

The final ultramylonite microstructure of fine equant to elongated grains with smooth boundaries is completely recrystallized. The EBSD map of the ultramylonite shows that the elongated olivine domains are polycrystalline suggesting that olivine dynamically recrystallized. If the olivine grain size was controlled by recrystallization, then maximum stress levels of about 400 MPa (van der Wal et al., 1993) are implied for olivine with a low water content. Such a high stress level may not have been appropriate for the entire history of movement, since a small grain size, once developed, may be stabilized by the high second-phase content present in the ultramylonite zone (Olgaard, 1991; Warren and Hirth, 2006).

It is also possible that the initial stage of grain size reduction did not occur by dynamic recrystallization. For instance, ultramylonites from the Balmuccia peridotite have a similar CPO, mineralogy, and microstructures to that found in our samples but the Balmuccia ultramylonites formed by ductile reactivation of pseudotachylites

(Ueda et al., 2008). Although no evidence has been found in the Pyrenean peridotites to suggest that the vein-like ultramylonites were initially formed as pseudotachylites, their narrow width could be explained by ductile reactivation of healed cataclastic fractures, as the ultramylonites have similar orientations to brittle planar discontinuities that developed throughout the Lers peridotite (Vissers et al., 1997). Some of the grain size reduction must also have occurred by phase transformations (Newman et al., 1999).

The step-wise decrease of grain size in the bands at the margin of the ultramylonite zone is remarkable. If the grain-size reduction is produced by dynamic recrystallization and/or phase transformation then formation of the bands in several distinct stages is indicated, with a concomitant decrease in the shear zone width with time.

The CPOs of olivine in the wall rock lherzolites are relatively strong and indicate that intracrystalline creep was the major mechanism of deformation on the (010) [100] slip system. The fact that the textures have an orthorhombic symmetry may indicate strong displacement partitioning or very high shear strains. The olivine porphyroclast CPO is somewhat different from the CPO in the wall rock. There is a [010] maximum parallel to the [010] CPO in the foliated lherzolite (compare Fig. 3a with b), and a [100] point maximum parallel to the [100] in the lherzolite (compare Fig. 3a with b). Most of the olivine clasts are elongated sigma clasts (Fig. 4E, F), which have a low rotation rate compared to their recrystallization rate (Passchier and Trouw, 1996), so the clast CPO is probably inherited from the initial CPO in the foliated wall rock.

The olivine and orthopyroxene grains in the ultramylonite bands are highly elongated suggesting either intragranular deformation and/or diffusive mass transfer. The absence of lattice bending and lack of subgrains in olivine grains implies that intragranular dislocation creep was limited. The extended olivine-orthopyroxene boundaries aligned sub-parallel to the shear zone boundary may act as sliding surfaces, but these boundaries have many low amplitude cusps along them (Fig. 6). The cusp-like geometry may be related to migration of the phase boundaries (Gower and Simpson, 1992; Sundberg and Cooper, 2008), which requires long-range diffusive transport of some elements. Any sliding along such irregular surfaces can only occur if sliding is accommodated by diffusion or local dislocation motion, although it is also possible that the cusps developed after deformation. The homogeneous distribution of phases and the lack of distinct compositional banding derived from olivine and pyroxene porphyroclasts also suggests significant mixing of phases by grain neighbor switching events (Bouillier and Guegen, 1975; Stunitz and Fitz Gerald, 1993; Newman et al., 1999). The microstructures are consistent with deformation by sliding along olivine-orthopyroxene boundaries accommodated by diffusive mass transfer and interface migration.

It is uncertain if the ultramylonites had wet or dry rheology. The occurrence of dolomite and amphibole indicates that the fluid was a CO_2 rich CHO fluid. The high CO_2 content of the fluid means water activity could be low, resulting in an effectively dry rheology (Ueda et al., 2008; Chernak et al., 2009). In addition water solubility in olivine is low at the PT conditions estimated for the ultramylonites. The CPO of the larger matrix grains in the ultramylonite is similar to the type B-CPO, which has been proposed by Jung and Karato (2001) to indicate moderate water content in olivine. However, more recent experiments (Sundberg and Cooper, 2008; Jung et al., 2009) have shown that type B CPO can also develop in completely dry olivine. In the case of the Lers ultramylonite studied here, a type B-CPO is only present in some bands of the ultramylonite and this local CPO could simply be inherited from the host grains in the foliated lherzolite that had [001] at a low angle to the shear direction (Fig. 3A).

Rheological regime maps for olivine based on experimental flow laws are useful in the analysis of the deformation mechanisms in natural mantle rocks (Karato et al., 1986; Rutter and Brodie, 1988; Drury and Fitz Gerald, 1998; Hirth, 2002; Drury, 2005). As water activity in the shear zones is likely to be low, we only consider rheological regime maps for dry olivine at 600 °C constructed from the flow laws of Hirth and Kohlstedt (2003) (Fig. 10), which is an appropriate temperature for crustal emplacement of the peridotite bodies. The map shows that dry olivine, with an average 2–3 μm grain size and at stresses less than 400 MPa, will deform dominantly by GSS (grain size sensitive) linear creep. If stress levels near the maximum possible stress occur, then deformation is predicted to occur close to the field boundary between the rheological GSS linear creep regime and the GSS-power law creep regime; however this maximum stress is estimated from the smallest grain size in the polycrystalline olivine. Most olivine grains in our samples have a larger grain size, which suggests lower stresses than 400 MPa. Thus deformation conditions were dominantly in the GSS linear creep regime, which is consistent with the mechanisms inferred from the microstructures. Rheological regime maps for wet olivine, also indicate dominant GSS linear creep under similar conditions (Drury, 2005).

4.4. CPO development

The occurrence of a CPO in the ultra-fine grained vein-like ultramylonites from Lers is unexpected, because the microstructures and highly mixed nature of the phases indicate that grain boundary sliding (GBS), probably accommodated by diffusion, was the most likely deformation mechanism. In experimental studies on olivine rocks (Karato, 1988; Fliervoet et al., 1999; McDonnell et al., 1999; Kellerman Slotemaker et al., 2004) a random, or

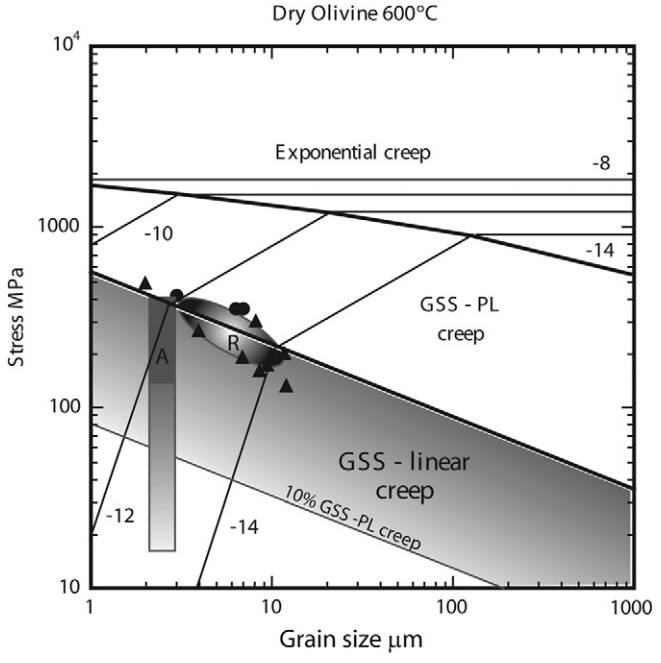

Fig. 10. Deformation mechanism map constructed for a temperature of 600 °C showing regimes for exponential creep, grain size sensitive (GSS) power law creep and grain size sensitive linear creep. The shaded area shows the conditions where more than 10% of the strain is accommodated by GSS-power law creep in the GSS linear creep regime. The triangles and squares are experimental data for dynamic recrystallized grain size in olivine. The ellipse (R) shows the estimated stress level based on the size of olivine grains in Fig. 8. Box A shows the ranges of stress and strainrate expected for an average grain size of 2–3 μm.

weak, olivine CPO is developed when grain boundary sliding and diffusive mass transfer dominate deformation. However, recent high strain experimental studies, on olivine-orthopyroxene rocks (Sundberg and Cooper, 2008) and feldspars (Heidelbach et al., 2000; Gomez Barreiro et al., 2007) have demonstrated that significant CPO can develop during deformation during GSS linear creep. It has been known for some time that modest CPO development occurs in calcite deformed in the intermediate GSS-power law creep regime (Rutter et al., 1994; Casey et al., 1998). The following models may account for the development or preservation of a CPO during GSS deformation.

4.4.1. CPO development by dislocation accommodated grain boundary sliding

When deformation occurs by GBS accommodated by dislocation motion, then, at high strains, the dislocation creep component may result in significant CPO development (Rutter et al., 1994), particularly in the larger grains. The type of CPO produced by the dislocation accommodated GBS creep deformation will vary with stress, temperature and water content and should be similar to the CPO developed by dominant dislocation creep, as the easy slip systems would be the same in both cases (Gomez Barreiro et al., 2007).

In olivine dislocation accommodated GBS is thought to occur in the GSS-power law rheological regime, which has a high stress exponent, and involves significant dislocation activity and grain size reduction by dynamic recrystallization (Hirth and Kohlstedt, 1995; Bystricky et al., 2000). CPO development in olivine is variable in the GSS-power law regime (Hirth and Kohlstedt, 1995). In experiments at a high temperature (1300 °C) a strong CPO is developed (Zhang et al., 2000) while at a lower temperature (1200 °C) larger grains have a strong CPO (Lee et al., 2002; Bystricky et al., 2000) and smaller, recrystallized grains have a random to weak CPO (Lee et al., 2002). The recrystallized grains formed at 1200 °C may have deformed by dominant grain boundary sliding and diffusion creep (Lee et al., 2002). Olivine rocks deformed to high strains under conditions close to the GSS-power law and GSS linear creep boundary, also have a weak CPO (Sundberg and Cooper, 2008). Precigout et al. (2007) have described a natural example of CPO probably formed in the olivine GSS-power law creep regime mylonites from the Ronda massif, Spain (van de Wal and Vissers, 1996). The CPOs in these Ronda mylonites are strong and consistent with easy slip on [100] (010).

The microstructures (Fig. 6) and estimated deformation conditions in the Lers ultramylonite (Fig. 10) are consistent with dominant grain/phase boundary sliding and diffusion creep, which implies that dislocation accommodated grain boundary sliding is unlikely to be the mechanism of CPO development in these rocks. However, the rheological regime map in Fig. 10 shows that there is a broad transition zone in the GSS linear regime, where the strainrate of GSS-power law creep is more than 10% of the strainrate due to GSS linear creep. In this transition zone it is possible that the dislocation activity, especially in larger grains would result in the development of CPO if strains are large enough. We note, however, that the orthopyroxene CPO (Fig. 8) is not consistent with simple shear deformation on the orthopyroxene easy slip system [001] (100) (Avé Lallemant, 1978).

4.4.2. CPO development during interface controlled diffusion creep

Sundberg and Cooper (2008) have shown that strong CPOs are formed in orthopyroxene-rich peridotites deforming to large strains in the GSS linear creep regime. The microstructures in Sundberg and Cooper's experiments are strikingly similar to the Lers ultramylonites, with elongated olivine and orthopyroxene grains and no subgrain development in either mineral. The experimental olivine CPO has a [010] maximum normal to the foliation and a [001] maximum parallel to the shear direction. Orthopyroxene [001] is also parallel to the shear direction. CPO strength increases in these experiments with an increase in orthopyroxene content. Sundberg and Cooper (2008) suggest that CPO development is produced by interface reaction control of diffusion along olivine-orthopyroxene phase boundaries. In this case dissolution and precipitation kinetics will depend on grain orientations (Tullis, 1989). Sundberg and Cooper (2008) further suggest that grain rotation and GBS processes result in grain orientations and boundary structures that yield the fastest creep rate. CPO in the GSS creep regime may also develop by rotation of elongated grains whose shape is crystallographically controlled (Bons and den Brok, 2000). The Lers ultramylonites are orthopyroxene rich and the CPO in the larger elongated grains is similar to the CPO in Sundberg and Cooper's (2008) experiments, although, in the Lers samples there is no consistent [001] maximum parallel to the shear direction for either olivine nor for orthopyroxene. These differences could be partly explained if the Lers ultramylonites are transpressional shear zones. In that case the olivine [001] maximum developed in simple shear (Sundberg and Cooper, 2008) could be replaced by an [001] and [100] girdle in the foliation plane.

4.4.3. Inherited-ghost CPO

The CPO in the ultramylonite zone may have been formed during early dislocation creep deformation and preserved during later GSS flow (Jiang et al., 2000; Casey et al., 1998; Casey and McGrew, 1999; Warren and Hirth, 2006). This mechanism will produce a variable CPO because the local CPO is controlled by the host orientation of the initial grains. Skemer and Karato (2008) have shown a good example of this type of CPO in orthopyroxene, deformed by GSS creep from kimberlite xenoliths. In the Lers ultramylonites the elongated shapes of larger grains may be important in the preservation of an initial CPO. Elongated flattened grains sliding over each other are not able to rotate about axes at low angles to the foliation plane. In contrast flattened elongated grains may rotate around axes at a high angle to the foliation, so the [010] maximum would be preserved and the [100] and [001] maxima would be dispersed along girdles, as observed in the ultramylonites in our work. This suggestion is supported by the recent numerical modeling study of Wheeler (2009) who showed that elongated grain shapes reduce the rate of grain rotation during deformation by GBS accommodated by diffusion.

4.4.4. Summary: CPO development

To summarize, the CPOs of the Lers ultramylonites are a natural example of olivine CPO preservation and/or CPO development during deformation by GBS and diffusive mass transfer. The olivine CPO in the ultramylonite matrix can be explained by a minor component of dislocation accommodated GBS, by the ghost-CPO model or by interface controlled diffusion creep in an orthopyroxene-rich rock composition.

4.5. Comparsion with other peridotite mylonites

In almost all previous studies of peridotite mylonites with grain sizes less than 15 μm, a random to very weak CPO has been found (Kleinschrodt, 1994; Newman et al., 1999; Michibayashi and Mainprice, 2004; Dijkstra et al., 2002; Warren and Hirth, 2006; Toy et al., 2010). Newman et al. (1999) were the first to report a weak to random olivine CPO in ultramylonites from the Turon de la Tecouere peridotite in the Western Pyrenees. In these ultramylonites there is a weak [100] maximum perpendicular to the lineation, which could have formed during diffusion accommodated grain/phase boundary sliding (Newman and Drury, 2010). Toy et al. (2010) have shown that olivine CPOs in an ultramylonite

zone from the Twin Sisters massif, Washington, USA, formed at 650–750 °C, vary with grain size and pyroxene content. Most olivine CPOs in these ultramylonites are very weak to random, with the exception of some weak olivine CPOs developed in pyroxene rich layers. Significant Opx CPO occurs in the Twin sisters ultramylonites, but as found in the Lers ultramylonite (Fig. 7), Toy et al. (2010) noted that the opx CPOs were not exactly the same as found in the experiments of Sundberg and Cooper (2008). The ultramylonite zones in the Balmuccia peridotite, which are re-activated pseudotachylite veins (Obata and Karato, 1995; Ueda et al., 2008) have similar microstructures and grain sizes (2 μm) as the Lers ultramylonites. Ueda et al. (2008) reported a weak but clear CPO, which they interpreted as evidence for dislocation creep. We suggest that the CPO in the Balmuccia ultramylonites could also be another example of CPO that developed during GSS linear creep.

4.6. Extrapolation to upper mantle conditions

Further studies are needed to investigate the deformation conditions and rock compositions that favor the preservation and/or development of CPO during GSS linear creep. The Lers vein-like ultramylonites were formed at low temperature and shallow depth during exhumation, most likely by reactivation of brittle structures (Vissers et al., 1997). As such they may not be representative of deeper level shear zones in the upper mantle, which have larger grain sizes and were deformed at higher temperatures and pressures (Vissers et al., 1991; Dijkstra et al., 2004; Precigout et al., 2007). However, if the olivine CPO in the Lers ultramylonites is related to the high orthopyroxene content (Sundberg and Cooper, 2008), then similar CPOs may occur in pyroxene rich mantle domains. GSS linear creep may be important in the deep upper mantle (Karato and Wu, 1993) at depths of 200–410 km, which has a much lower seismic anisotropy than the shallow mantle. Deep mantle peridotites have high pyroxene contents and many olivine-pyroxene boundaries (Drury and Fitz Gerald, 1998), thus CPO development (Sundberg and Cooper, 2008) or preservation from an earlier deformation (Wheeler, 2009) could be important in the deep upper mantle. In consequence, we suggest that a variety of weak CPOs, including the "type B-CPO", with a fast seismic direction perpendicular to direction of flow, could develop in the deeper mantle. We acknowledge that this suggestion is speculative and that further research is needed on the effect of pyroxene content, grain size and deformation conditions on CPO development.

5. Conclusions

1) Thin 2–10 mm wide ultramylonite zones from the Étang de Lers lherzolite, Pyrenees, France, are ultra-fine grained (0.5–10 μm) rocks with significant amounts of dolomite and amphibole in the matrix and rare plagioclase grains at the rims of spinel porphyroclasts.
2) The ultramylonite zones contain bands that are parallel to the zone margin, where the grain size abruptly decreases toward the center of the zone.
3) The Lers ultramylonites have a weak CPO in the olivine and orthopyroxene grains, which varies in different bands and is stronger in the coarser (3–10 μm) olivine. The CPO has a systematic relationship to the foliation with an olivine [010] maximum normal to foliation.
4) The ultramylonite contains ultra-fine, equi-axed to elongated grains, no subgrains, phase boundary alignments and a mixed phase distribution. These microstructures suggest that the dominant deformation mechanism involved grain boundary sliding and diffusive mass transfer.
5) The discovery of these rocks confirms conclusions from recent experimental studies that significant CPO and seismic anisotropy can occur in naturally deformed mantle rocks deformed by grain boundary sliding and diffusion creep.

Acknowledgments

Virginia (Jinny) Sisson is thanked for her help with the production of the photomicrographs. Lori Kennedy and Elisabetta Mariani are thanked for constructive reviews. The Netherlands Research School for Integrated Solid Earth Sciences (ISES) is acknowledged for funding the fieldwork. The electron microscopy was conducted in EMU (Electron Microscopy Utrecht), Department of Biology, Utrecht University.

Appendix. Supplementary material

Supplementary material associated with this article can be found, in the online version, at doi:10.1016/j.jsg.2011.10.002.

References

Albarède, F., Michard-Vitrac, A., 1978. Age and significance of the North Pyrenean metamorphism. Earth and Planetary Science Letters 40, 327–332.
Avé Lallemant, H.G., 1967. Structural and petrofabric analysis of an "Alpine-type" peridotite: the Lherzolite of the French Pyrenees. Leidse Geologische Mededelingen 42, 1–57.
Avé Lallemant, H.G., 1975. Mechanisms of preferred orientations of olivine in tectonite peridotites. Geology 3, 653–656.
Avé Lallemant, H.G., 1978. Experimental deformation of diopside and websterite. Tectonophysis 48, 1–27.
Avé Lallemant, H.G., Carter, N.L., 1970. Syntectonic recrystallization of olivine and modes of flow in the upper mantle. Geological Society of America Bulletin 81 (8), 2203–2220.
Avé Lallemant, H.G., Oldow, J.S., 2000. Active displacement partitioning and arc-parallel extension of the Aleutian volcanic arc based on Global Positioning System geodesy and kinematic analysis. Geology 28 (8), 739–742.
Barruol, G., Souriau, A., Vauchez, A., Díaz, J., Gallart, J., Tubia, J., Cuevas, J., 1998. Lithospheric anisotropy beneath the Pyrenees from shear wave splitting. Journal of Geophysical Research 103 (B12), 30039–30053.
Ben Ismail, W., Mainprice, D., 1998. An olivine fabric database: an overview of upper mantle fabrics and seismic anisotropy. Tectonophysics 296, 145–157.
Bodinier, J.-L., Menzies, M.A., Shimizu, N., Frey, F.A., McPherson, E., 2004. Silicate, hydrous and carbonate metasomatism at Lherz, Frane: contemporaneous derivatives of silicate melt-harzburgite reaction. Journal of Petrology 45, 299–320.
Bons, P.D., den Brok, B., 2000. Crystallographic preferred orientation development by dissolution-precipitation creep. Journal Structural Geology 22, 1713–1722.
Bouiller, A.-M., Guegen, Y., 1975. SP-mylonites: origin of some mylonites by superplastic flow. Contributions Mineralogy and Petrology 50, 93–104.
Bucher, K., Frey, M., 1994. Petro-genesis of Metamorphic Rocks. Springer Verlag, Berlin.
Bystricky, M., Kunze, K., Burlini, L., Burg, J.-P., 2000. High shear strain of olivine aggregates: rheological and seismic consequences. Science 290, 1564–1567.
Carter, N.L., Avé Lallemant, 1970. High temperature flow of dunite and peridotite. Geological Society of America Bulletin 81 (8), 2181–2202.
Casey, M., McGrew, A.J., 1999. One-dimensional kinematic model of preferred orientation development. Tectonophysics 303, 131–140.
Casey, M., Kunze, K., Olgaard, D.L., 1998. Texture of solenhofen limestone deformed to high strains in torsion. Journal of Structural Geology 20, 255–267.
Casteras, M., 1933. Recherches sur la structure du versant nord des Pyrénées Centrales et Orientales. Bulletin des Services de la Carte Géologique de la France, 525.
Chernak, L.J., Hirth, G., Selverstone, J., Tullis, J., 2009. Effect of aqueous and carbonic fluids on the dislocation creep of quartz. Journal of Geophysical Research 114, B04201.
Chopra, P.N., Paterson, M.S., 1984. The role of water in the deformation of dunite. Journal of Geophysical Research 89, 7861–7876.
Choukroune, P., Seguret, M., 1973. Carte structurale des pyrenees. Elf-ERAP.
Choukroune, P., Roure, F., Pinet, B., ECORS Pyrenees team, 1990. Main results of the ECORS Pyrenees profile. Tectonophysics 173, 411–423.
Connolly, J.A.D., Trommsdorf, V., 1991. Petrogenetic grids for metacarboate rocks: pressure-temperature phase-projection for mixed-volatile systems. Contributions to Mineralogy and Petrology 108, 93–105.
Den Tex, E., 1969. Origin of ultramafic rocks, their tectonic setting and history: a contribution to the discussion of the paper "the origin of ultramafic and ultrabasic rocks" by P.J. Wyllie. Tectonophysics 7, 457–488.

Dijkstra, A.H., Drury, M.R., Vissers, R.L.M., Newman, J., 2002. On the role of melt-rock reaction in mantle shear zone formation in the Othris peridotite massif (Greece). Journal of Structural Geology 24, 1431–1450.

Dijkstra, A.H., Drury, M.R., Vissers, R.L.M., Newman, J., van Roermund, H.L.M., 2004. Shear zones in the upper mantle: evidence from alpine- and ophiolite-type peridotite massifs. In: Alsop, G.I., Holdsworth, R.E., McCaffrey, K.J.W., Hand, M. (Eds.), Flow Processes in Faults and Shear Zones. Special Publication Geological Society London, vol. 224, pp. 11–24.

Drury, M.R., 2005. Dynamic recrystallization and strain softening of olivine aggregates in the laboratory and the lithosphere. In: Gapais, D., Brun, J.-P., Cobbold, P.R. (Eds.), Deformation Mechanisms, Rheology and Tectonics from Minerals to the Lithosphere. Geological Society Special Publication, 243, pp. 143–158.

Drury, M.R., Fitz Gerald, J.D., 1998. Mantle rheology: insights from laboratory studies of deformation and phase transition. In: Jackson, I.N.S. (Ed.), The Earths Mantle, Composition, Structure and Evolution, pp. 503–559.

Fabriès, J., Lorand, J.-P., Bodinier, J.-L., 1998. Petrogenetic evolution of orogenic lherzolite massifs in the cenyral and western Pyrenees. Tectonophysics 292, 145–167.

Fabriès, J., Lorand, J.-P., Bodinier, J.-L., Dupuy, C., 1991. Evolution of the upper mantle beneath the Pyrenees: evidence from spinel lherzolite massif. Journal of Petrology, Special Lherzolite Issue, 55–76.

Faul, U.H., Fitz Gerald, J.D., 1999. Grain misorientations in partially molten olivine aggregates: an electron backscatter diffraction study. Physics and Chemistry of Minerals 26, 187–197.

Fettes, D., Desmons, J. (Eds.), 2007. Metamorphic Rocks: a Classification and Glossary of Terms. Recommendations of the International Union of Geological Sciences Subcommission on the Systematics of Metamorphic Rocks. Cambridge University Press, Cambridge.

Fliervoet, T.F., Drury, M.R., Chopra, P.N., 1999. Crystallographic preferred orientations and misorientations in some olivine rocks deformed by diffusion or dislocation creep. Tectonophysics 303, 1–27.

Golberg, J.M., Leyreloup, A.F., 1990. High temperature-low pressure Cretaceous metamorphism related to crustal thinning (Eastern North Pyrenean Zone, France). Contributions to Mineralogy and Petrology 104, 194–207.

Gomez Barreiro, J., Lonardelli, I., Wenk., H.R., Dresen, G., Rybacki, E., Ren, Y., Tome, C.N., 2007. Preferred orientation of anorthite deformed experimentally in Newtonian creep. Earth and Planetary Science Letters 264, 188–207.

Gower, R.J.W., Simpson, C., 1992. Phase boundary mobility in naturally deformed, high grade quartzofeldspathic rocks: evidence for diffusional creep. Journal of Structural Geology 14, 301–313.

Heidelbach, F., Post, A., Tullis, J., 2000. Crystallographic preferred orientation in albite deformed experimentally by dislocation and solution precipitation creep. Journal of Structural Geology 22, 1649–1661.

Henry, P., Azambre, B., Montigny, R., Rossy, M., Stevenson, R.K., 1998. Late mantle evolution of the Pyrenean sub-continental lithospheric mantle in the light of new ^{40}Ar-^{39}Ar and Sm-Nd ages on pyroxenites and peridotites (Pyrenees, France). Tectonophysics 296, 103–123.

Hirth, G., Kohlstedt, D.L., 1995. Experimental constraints on the dynamics of the partially molten upper mantle – deformation in the diffusion creep regime. Journal of Geophysical Research 100, 1981–2001.

Hirth, G., Kohlstedt, D.L., 2003. Rheology of the upper mantle and the mantle wedge: a view from the experimentalists. In: Eiler, J. (Ed.), The Subduction Factory. Geophysical Monographs, vol. 138. American Geophysical Union, Washington DC, pp. 83–105.

Hirth, G., 2002. Laboratory constraints on the rheology of the upper mantle. In: Karato, S.-I., Wenk, H.-R. (Eds.), Plastic Deformation of Minerals and Rocks, vol. 51. Reviews in Mineralogy & Geochemistry, pp. 94–120.

Iyer, K., Jamveit, B., Mathiesen, J., Malthe-Sorenssen, A., Feder, J., 2008. Reaction -assisted hierarchical fracturing during serpentinization. Earth and Planetary Science Letters 267, 503–516.

Jiang, Z., Prior, D.J., Wheeler, J., 2000. Albite crystallographic preferred orientation and grain misorientation distribution in low grade mylonite: implications for granular flow. Journal of Structural Geology 22, 1663–1674.

Jung, H., Karato, S., 2001. Water-induced fabric transitions in olivine. Science 293, 1460–1463.

Jung, H., Mo, W., Green, H.W., 2009. Upper mantle seismic anisotropy resulting from pressure-induced slip transition in olivine. Nature Geoscience 2, 73–77.

Karato, S.-I., 1988. The role of recrystallization in the preferred orientation of olivine. Physics of the Earth and Planetary Interiors 51, 107–122.

Karato, S.-I., Wu, P., 1993. Rheology of the upper mantle: a synthesis. Science 260, 771–778.

Karato, S.-I., Paterson, M.S., Fitz Gerald, J.D., 1986. Rheology of synthetic olivine grain aggregates: influence of grain size and water. Journal of Geophysical Research 91, 8151–8176.

Kellerman Slotemaker, A., de Bresser, J.H.P., Spiers, C.J., Drury, M.R., 2004. Microstructural evolution of synthetic forsterite aggregates deformed to high strain. Materials Science Forum 467-470, 579–584.

Kleinschrodt, R., 1994. Competing crystal pastic and grain size sensitive deformation mechanisms in a peridotite mylonite from the Finero complex (Ivrea Zone, NW Italy). In: Bunge., S., Siegesmund, H.J., Skrotzki, W., Weber, K. (Eds.), Textures of Geological Materials, pp. 203–220.

Lacroix, A., 1894. Étude minéralogique de la lherzolite des Pyrénées et de ses phénomènes de contact. In: Nouvelles Archives de Museum de Histoire Naturelle, series 3, vol. 6 209–308.

Lagabrielle, Y., Bodinier, J.-L., 2008. Submarine reworking of exhumed subcontinental mantle rocks: field evidence from the lherz peridotites, French Pyrenees. Terra NovaERY 20, 11–21.

Lagabrielle, Y., Labaume, P., de Saint Blanquart, M., 2010. Mantle exhumation, crustal denudation, and gravity tectonics during Cretaceous rifting in the Pyrenean realm (SW Europe): insights from the geological setting of the lherzolite bodies. Tectonics 29, TC4012.

Larrasoaña, J.C., Parés, J.M., Millán, H., Del Valle, J., Pueyo, E.L., 2003. Paleomagnetic, structural, and stratigraphic constraints on transfer fault kinematics during basin inversion: the Pamplona Fault (Pyrenees, north Spain). Tectonics 22 (6), 1071. doi:10.1029/2002TC001447.

Le Roux, V., Bodinier, J.-L., Tomasi, A., Alard, O., Dautria, J.-M., Vauchez, A., Riches, A.J.V., 2007. The lherz spinel lherzolite: refertilized rather than pristine mantle. Earth and Planetary Science Letters 259, 599–612.

Le Roux, V., Tommasi, A., Vauchez, A., 2008. Feedback between melt percolation and deformation in an exhumed lithosphere asthenosphere boundary. Earth and Planetary Science Letters 274, 401–413.

Lee, K.-H., Jiang, Z., Karato, S.-I., 2002. A scanning electron microscope study of the effects of dynamic recrystallization on lattice preferred orientation in olivine. Tectonophysics 351, 331–341.

Mainprice, D., Nicolas, A., 1989. Development of shape and lattice preferred orientations: applications to the seismic anisotropy of the lower crust. Journal of Structural Geology 11, 175–189.

McDonnell, R.D., Peach, C.J., Spiers, C.J., 1999. Flow behavior of fine-grained synthetic dunite in the presence of 0.5 wt% H_2O. Journal of Geophysical Research 104, 17823–17845.

Michibayashi, K., Mainprice, D., 2004. The role of pre-exiting mechanical anisotropy on shear zone development within oceanic lithosphere: an example from the Oman ophiolite. Journal of Petrology 45, 405–411.

Minnigh, L.D., van Calsteren, P.W.C., den Tex, E., 1980. Quenching: an additional model for the emplacement of the lherzolite at Lers (French Pyrenees). Geology 8 (1), 18–21.

Newman, J., Drury, M.R., 2010. Control of shear zone location and thickness by initial grain size variations in upper mantle peridotites. Journal of Structural Geology 32, 832–842.

Newman, J., Lamb, W.M., Drury, M.R., Vissers, R.L.M., 1999. Deformation processes in a peridotite shear zone: reaction-softening by an H2O-deficient, continuous net transfer reaction. Tectonophysics 303, 193–222.

Nicolas, A., 1986. Structure and petrology of peridotites: clues to their geodynamic environment. Reviews of Geophysics 24, 875–895.

Obata, M., Karato, S.-I., 1995. Ultramafic pseudotachylite from the Balmuccia peridotite, Ivrea-Verbano zone, Northen Italy. Tectonophysics 242, 313–328.

Olgaard, D.L., 1991. The role of second phase in localizing deformation. In: Knipe, R.J., Rutter, E.H. (Eds.), Deformation Mechanisms, Rheology and Tectonics. Geological Society Special Publication, vol. 54, pp. 175–181.

Passchier, C.W., Trouw, R.A.J., 1996. Microtectonics. Springer Verlag, New York, 289 pp.

Precigout, J., Gueydan, F., Gapais, D., Garrido, C.J., Essasifi, A., 2007. Strain localization in the subcontinental mantle – a ductile alternative to the brittle mantle. Tectonophysics 445, 318–336.

Ravier, J., 1959. Le métamorphisme des terrains secondaires des Pyrénées. In: Mémoires de la Société géologique de France, nouvelle series, 38/86, 250 pp.

Rutter, E.H., Casey, M., Burlini, L., 1994. Preferred crystallographic orientation development during the plastic and superplastic flow of calcite rocks. Journal of Structural Geology 16, 1421–1446.

Rutter, E.H., Brodie, K., 1988. The role of grainsize reduction in the rheological stratification of the lithosphere. Geologische Rundschau 77, 295–308.

Sibuet, J.-C., Srivastava, S.P., Spakman, W., 2004. Pyrenean orogeny and plate kinematics. Journal of Geophysical Research 109 (B8), B08104. doi:10.1029/2003JB002514.

Skemer, P., Karato, S.I., 2008. Sheared lherzolite xenoliths revisited. Journal of Geophysical Research 113, B07205.

Stunitz, H., Fitz Gerald, J.D., 1993. Deformation of granitoids at low metamorphic grade: 2 Granular flow in albite rich mylonites. Tectonophysics 221, 299–324.

Sundberg, M., Cooper, R.F., 2008. Crystallographic preferred orientation produced by diffusional creep of harzburgite: effects of chemical interactions among phases during plastic flow. Journal of Geophysical Research 113, B12208.

Toy, V.G., Newman, J., Lamb, W., Tikoff, B., 2010. The role of pyroxenites in formation of shear instabilities in the mantle: evidence from an ultramafic ultramylonite, Twin Sisters massif, Washington. Journal of Petrology 51, 55–80.

Trommsdorf, V., Connolly, J.A.D., 1990. Constraints on phase diagram topology for the system $CaO–MgO–SiO_2–CO_2–H_2O$. Contributions to Mineralogy and Petrology 104, 1–7.

Tullis, T.E., 1989. Development of preferred orientation due to anisotropic dissolution/growth rates during solution transfer creep. EOS Transactions, American Geophysical Union 70, 457–458.

Ueda, T., Obata, M., Di Toro, G., Kanagawa, K., Ozawa, K., 2008. Mantle earthquakes frozen in mylonitized ultramafic pseudotachylytes of spinel-lherzolite facies. Geology 36, 607–610.

van de Wal, D., Vissers, R.L.M., 1996. Structural petrology of the Ronda peridotite, SW Spain: deformation history. Journal of Petrology 37, 23–43.

Van der Voo, R., Boessenkool, A., 1973. Permian paleomagnetic result from the western Pyrenees delineating the plate boundary between the Iberian Peninsula and stable Europe. Journal of Geophysical Research 78 (23), 5118–5127.

van der Wal, D., Chopra, P.N., Drury, M.R., Fitz Gerald, J.D., 1993. Recrystallised grain-size stress relationships in experimentally deformed olivine-rocks. Geophysical Research Letters 20, 1479–1482.

Vera, J.-A., 2001. Evolution of the South Iberian continental margin. In: Ziegler, P.A., Cavazza, W., Robertson, A.H.F., Crasquin-Soleau, S. (Eds.), Peri-tethys Memoir 6: Pery-Tethyan Rift/Wrench Basins and Passive Margins, vol. 186. Mémoires Muséum National d'Histore Naturelle, pp. 109–143.

Vergés, J., García Senz, J.M., 2001. Mesozoic evolution and cenozoic inversion of the Pyrenean rift. In: Ziegler, P.A., Cavazza, W., Robertson, A.H.F., Crasquin-Soleau, S. (Eds.), Peri-tethys Memoir 6: Pery-Tethyan Rift/Wrench Basins and Passive Margins, vol. 186. Mémoires Muséum National d'Histore Naturelle, pp. 187–212.

Vissers, R.L.M., Drury, M.R., Hoogerduijn Strating, E.H., Van der Wal, D., 1991. Shear zones in the upper mantle; a case study from an Alpine lherzolite. Geology 19, 990–993.

Vissers, R.L.M., Drury, M.R., Newman, J., Fliervoet, T.F., 1997. Mylonitic deformation in upper mantle peridotites of the North Pyrenean Zone (France): implications for strength of strain localization in the lithosphere. Tectonophysics 279, 303–325.

Vissers, R.L.M., 1992. Variscan extension in the Pyrenees. Tectonics 11 (6), 1369–1384.

Walker, A.N., Rutter, E.H., Brodie, K.H., 1990. Experimental study of grain-size sensitive flow of synthetic, hot-pressed calcite rocks. In: Knipe, R.J., Rutter, E.H. (Eds.), Deformation Mechanisms, Rheology and Tectonics, vol. 54. Geol. Soc. Spec. Pub, pp. 259–284.

Warren, J.M., Hirth, G., 2006. Grain size sensitive deformation mechanisms in naturally deformed peridotites. Earth and Planetary Science Letters 248, 423–435.

Weil, A.B., Van der Voo, R., van der Pluijm, B.A., 2001. Oroclinal bending and evidence against the Pangea megashear: the Cantabria-Asturias arc (northern Spain). Geology 29 (11), 991–994.

Wheeler, J., 2009. The preservation of seismic anisotropy in the Earth's mantle during diffusion creep. Geophysical Journal of the International 178, 1723–1732.

Woodland, A.B., Kornprbst, J., McPherson, E., Bodinier, J.-L., Menzies, M.A., 1996. Metasomatic interactions in the lithospheric mantle: petrological evidence from the Lherz massif, French Pyrenees. Chemical Geology 134, 83–112.

Wyllie, P.J., 1979. Magmas and volatile components. American Mineralogist 64, 469–500.

Yaxley, G.M., Crawford, A.J., Green, D.H., 1991. Evidence for carbonatite metasomatism in spinel peridotite xenoliths from western Victoria, Australia. Earth and Planetary Science Letters 107, 305–317.

Yilmaz, P.O., Norton, I.O., Leary, D., Chuchla, R.J., 1996. Tectonic evolution and paleogeography of Europe. In: Ziegler, P.A., Horvàth, F. (Eds.), Peri-thetis Memoir 2: Structure and Prospects of Alpine Basins and Forelands. Muséum National d'Histoire Naturelle, Publications Scientifiques, Paris, France, pp. 47–60.

Zhang, S., Kararo, S.-I., 1995. Lattice preferred orientation of olivine aggregates deformed in simple shear. Nature 375, 774–777.

Zhang, S., Karato, S.-I., Fitz Gerald, J.D., Faul, U.H., Zhou, Y., 2000. Simple shear deformation of olivine aggregates. Tectonophysics 316, 133–152.

Zwart, H.J., 1962. On the determination of polymetamorphic mineral associations, and its application to the Bosost area (Central Pyrenees). Geologische Rundschau 52, 38–65.